Electronic Supplementary Material (ESI) for Dalton Transactions

Syntheses, characterizations and properties of $[Mo_2O_2S_2]$-based oxothiomolybdenum wheels incorporating bisphosphonate ligands.

Hani El Moll,[a] Justin Claude Kemmegne-Mbouguen,[a,b] Mohamed Haouas,*[a] Francis Taulelle,[a] Jérôme Marrot,[a] Emmanuel Cadot, Pierre Mialane, Sébastien Floquet,*[a] and Anne Dolbecq*[a]

a) Institut Lavoisier de Versailles, UMR 8180, Université de Versailles Saint-Quentin en Yvelines, 45 avenue des Etats-Unis, 78035 Versailles, France. E-mails: dolbecq@chimie.uvsq.fr, sebastien.floquet@chimie.uvsq.fr, haouas@chimie.uvsq.fr .

b) Laboratoire de Chimie Analytique, Faculté des Sciences, Université de Yaoundé I, B.P. 812, Yaoundé, Cameroon

Supporting Information

Table SI1. Comparison of selected bond distances in **$Mo_8S_8(Ale)_4$**, **$Mo_8S_8(Zol)_4$** and **$Mo_8O_8(Ale)_4$**.

$Mo_8S_8(Ale)_4$		**$Mo_8S_8(Zol)_4$**		**$Mo_8O_8(Ale)_4$**			
Mo(1)-O(1)	1.6906(11)	Mo(1)-O(1)	1.677(3)	Mo(1)-O(1)	1.681(4)	Mo(5)-O(25)	1.704(4)
Mo(1)-O(2)	2.0698(11)	Mo(1)-O(2)	2.130(4)	Mo(1)-O(2)	1.932(4)	Mo(5)-O(9)	1.944(4)
Mo(1)-O(3)	2.1058(11)	Mo(1)-O(3)	2.200(3)	Mo(1)-O(3)	1.946(4)	Mo(5)-O(8)	1.948(4)
Mo(1)-S(1)	2.3219(4)	Mo(1)-O(4)	2.204(3)	Mo(1)-O(4)	2.074(4)	Mo(5)-O(26)	2.057(4)
Mo(1)-S(2)	2.3226(4)	Mo(1)-S(2)	2.3263(14)	Mo(1)-O(5)	2.079(4)	Mo(5)-O(27)	2.110(4)
Mo(1)-O(4)	2.3924(10)	Mo(1)-S(1)	2.3295(15)	Mo(1)-O(6)	2.408(4)	Mo(5)-O(28)	2.287(4)
Mo(1)-Mo(2)	2.8387(2)	Mo(1)-Mo(1)	2.8525(8)	Mo(1)-Mo(6)	2.5834(7)		
						Mo(6)-O(29)	1.705(5)
Mo(2)-O(5)	1.6832(11)	Mo(2)-O(5)	1.679(4)	Mo(2)-O(7)	1.681(4)	Mo(6)-O(2)	1.934(4)
Mo(2)-O(6)	2.1032(10)	Mo(2)-O(7)	2.109(3)	Mo(2)-O(8)	1.938(4)	Mo(6)-O(3)	1.941(4)
Mo(2)-O(7)	2.1074(10)	Mo(2)-O(6)	2.111(4)	Mo(2)-O(9)	1.942(4)	Mo(6)-O(30)	2.045(4)
Mo(2)-S(1)	2.3243(4)	Mo(2)-S(3)	2.3078(17)	Mo(2)-O(10)	2.072(4)	Mo(6)-O(31)	2.116(4)
Mo(2)-S(2)	2.3261(4)	Mo(2)-S(4)	2.3275(16)	Mo(2)-O(11)	2.092(4)	Mo(6)-O(32)	2.311(4)
Mo(2)-O(8)	2.3965(11)	Mo(2)-O(8)	2.402(3)	Mo(2)-O(12)	2.416(4)		
		Mo(2)-Mo(2)	2.8583(8)	Mo(2)-Mo(5)	2.5968(7)	Mo(7)-O(33)	1.695(4)
						Mo(7)-O(20)	1.929(4)
				Mo(3)-O(13)	1.703(4)	Mo(7)-O(21)	1.949(4)
				Mo(3)-O(15)	1.951(4)	Mo(7)-O(34)	2.100(4)
				Mo(3)-O(14)	1.952(4)	Mo(7)-O(35)	2.111(4)
				Mo(3)-O(16)	2.036(4)	Mo(7)-O(36)	2.358(4)
				Mo(3)-O(17)	2.129(4)		
				Mo(3)-O(18)	2.310(4)	Mo(8)-O(37)	1.692(4)
				Mo(3)-Mo(8)	2.5921(7)	Mo(8)-O(14)	1.942(4)
						Mo(8)-O(15)	1.950(4)
				Mo(4)-O(19)	1.702(4)	Mo(8)-O(38)	2.071(4)
				Mo(4)-O(20)	1.937(4)	Mo(8)-O(39)	2.076(4)
				Mo(4)-O(21)	1.951(4)	Mo(8)-O(40)	2.413(4)
				Mo(4)-O(23)	2.056(4)		
				Mo(4)-O(22)	2.090(4)		
				Mo(4)-O(24)	2.357(4)		
				Mo(4)-Mo(7)	2.5758(7)		

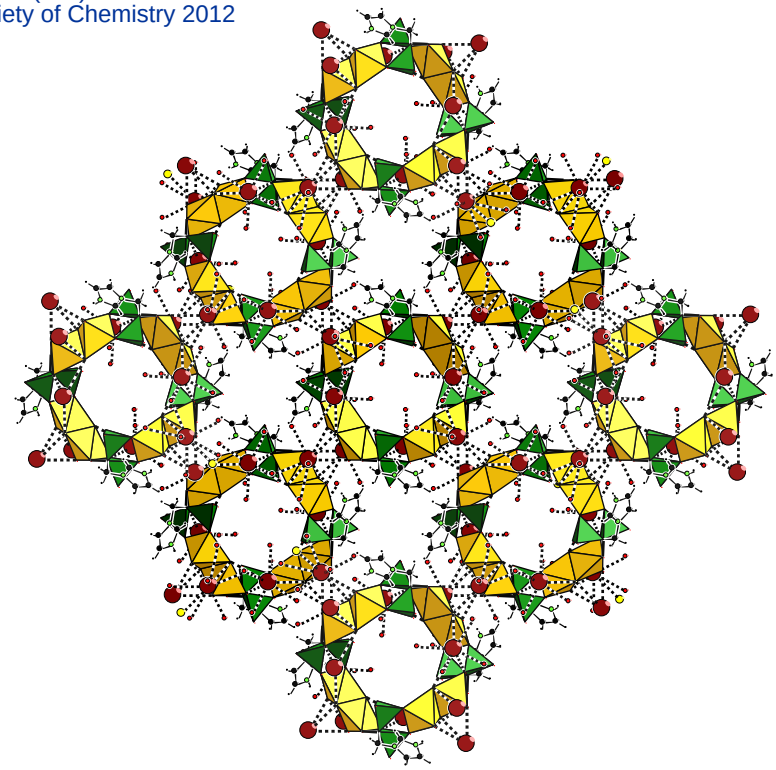

(a)

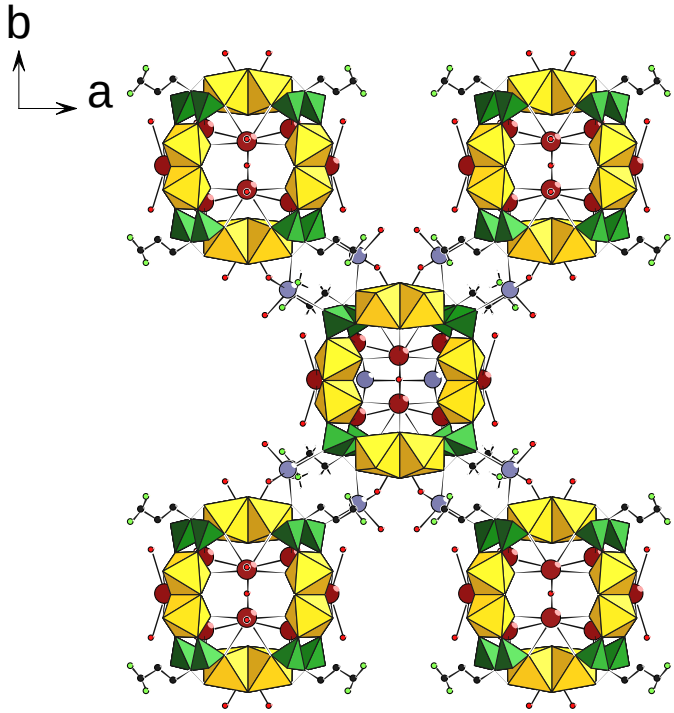

Figure SI1: View along the *c* axis of the 3D structure of (a) Rb_8**Mo_8S_8(Zol)$_4$**$.32H_2O$ and (b) $Rb_{4.75}K_{3.25}$**Mo_8S_8(Ale)$_4$**$.25H_2O$; brown spheres = Rb, blue spheres = K, red spheres = O, green spheres = N, black spheres = C, yellow octahedra = MoO_2S_2, green tetrahedra = PCO_3.

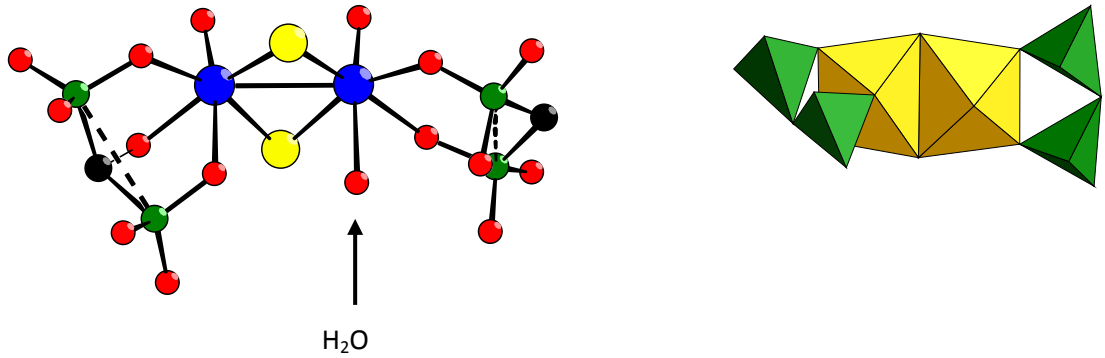

$Mo_8S_8(Zol)_4$

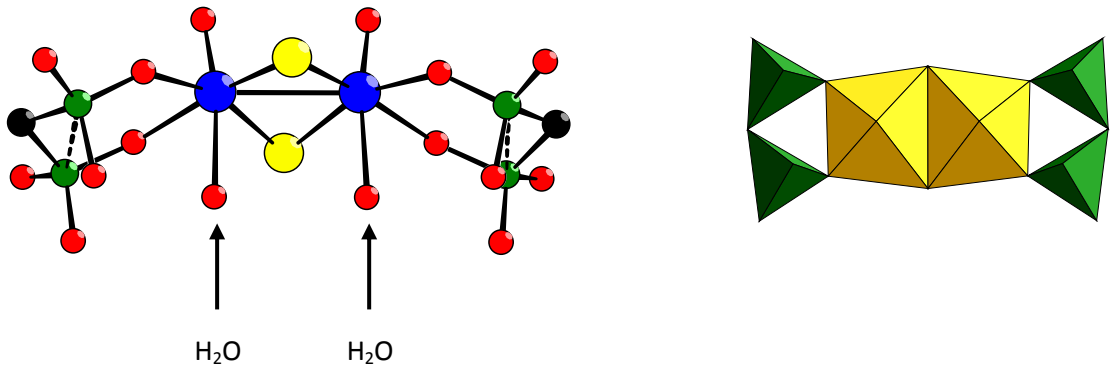

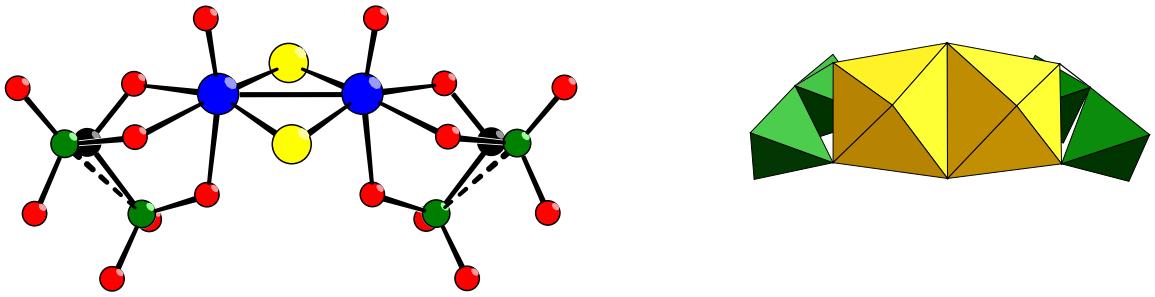

$Mo_8S_8(Ale)_4$

Figure SI2: View of (a) a $\{Mo^{V}_2S_2O_2\}^{2+}$ dimer with BP ligands connected symmetrically in **$Mo_8S_8(Zol)_4$** and (b) the two kinds of Mo^{V} dimers with BP ligands connected dissymmetrically in **$Mo_8S_8(Ale)_4$**; red spheres = O, blue spheres = Mo, green spheres = P, **black spheres = C, yellow octahedra = MoO_2S_2, green tetrahedra** = PCO_3.

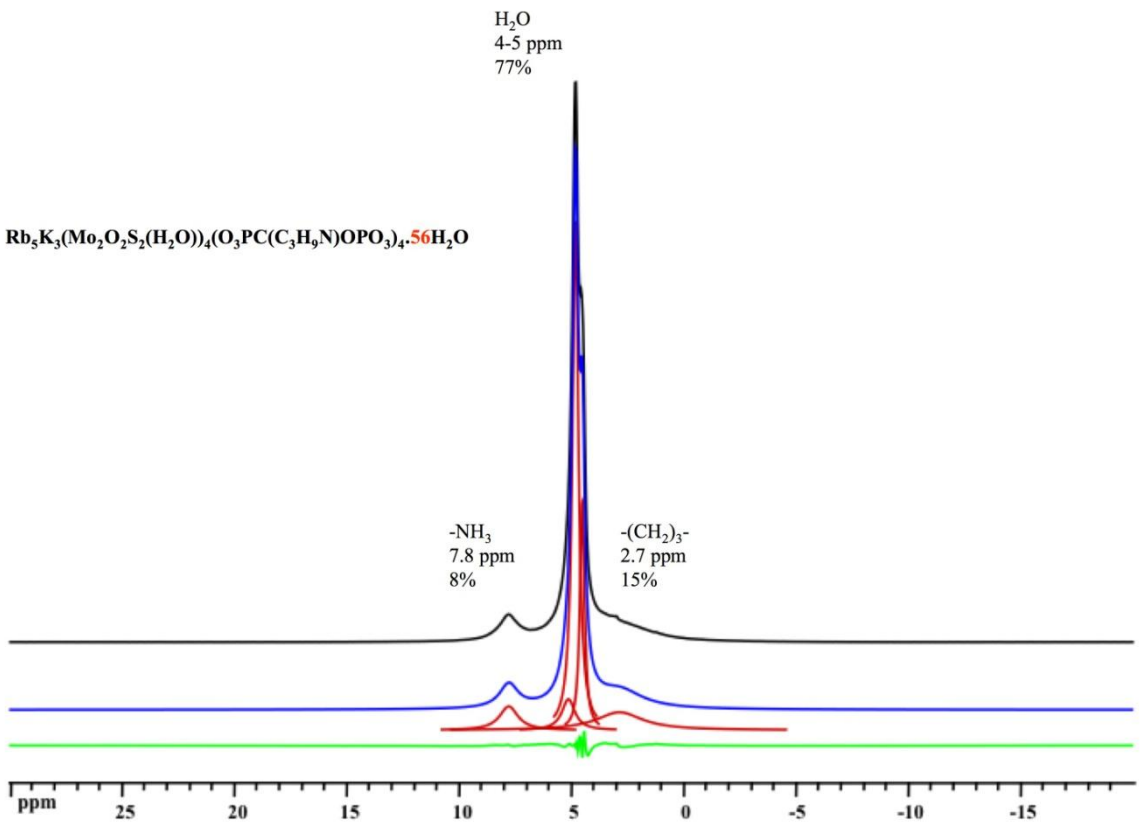

Figure SI3: Experimental ^{1}H MAS NMR spectrum (black line) and simulated spectrum (blue line) with the decomposition (red lines) and difference spectrum (green line) of **Mo_8S_8(Ale)$_4$.**

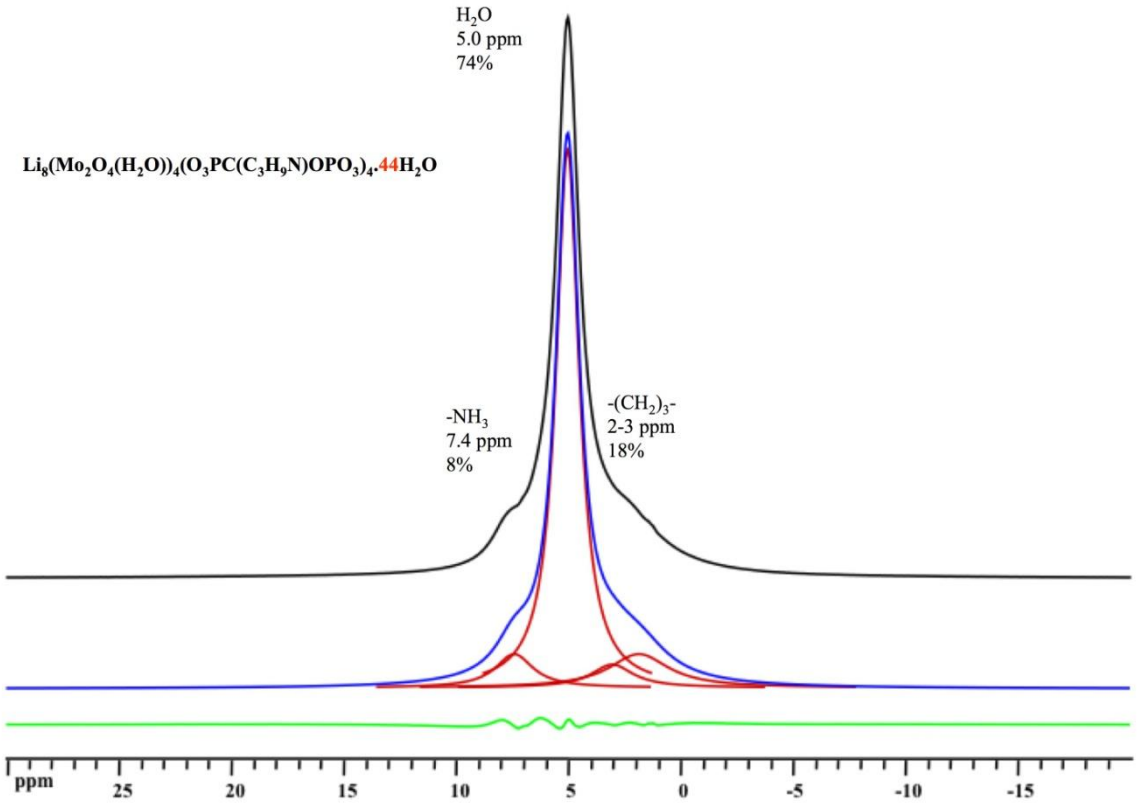

Figure SI4: Experimental ^{1}H MAS NMR spectrum (black line) and simulated spectrum (blue line) with the decomposition (red lines) and difference spectrum (green line) of **Mo_8O_8(Ale)$_4$.**

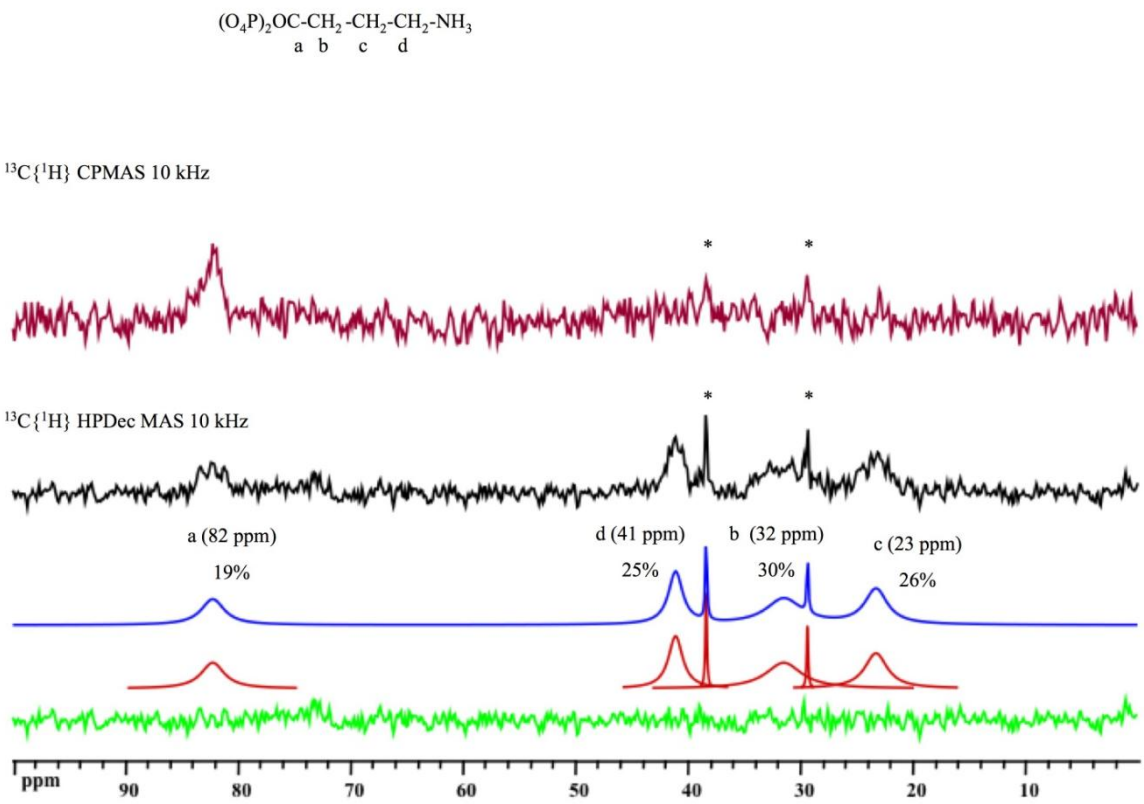

Figure SI5: Experimental $^{13}C\{^{1}H\}$ CPMAS (top) and MAS (bottom black line) NMR spectra and simulated spectrum (blue line) with the decomposition (red lines) and difference spectrum (green line) of **$Mo_8S_8(Ale)_4$** acquired under heteronuclear TPPM decoupling. Asterisks denote the signals of adamantane due to sample contamination in the NMR rotor.

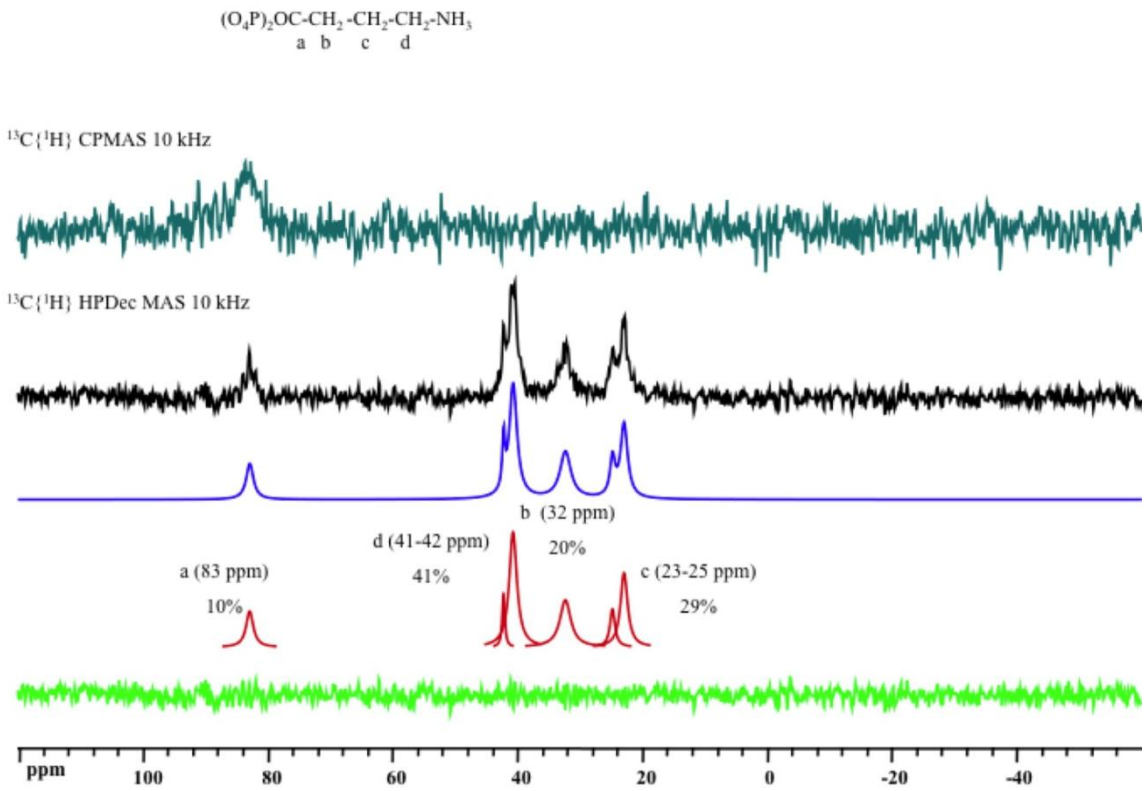

Figure SI6: Experimental $^{13}C\{^{1}H\}$ CPMAS (top) and MAS (bottom, black line) NMR spectra and simulated spectrum (blue line) with the decomposition (red lines) and difference spectrum (green line) of **$Mo_8O_8(Ale)_4$** acquired under heteronuclear TPPM decoupling.

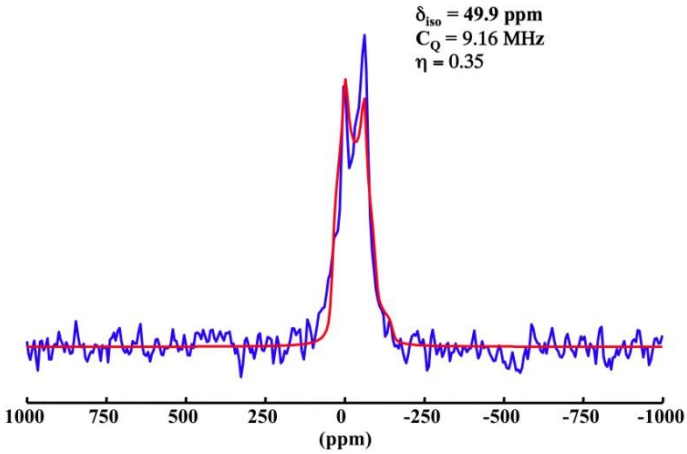

Figure SI7: Experimental ^{87}Rb MAS NMR spectrum (blue line) and simulated spectrum (red line) of **$Mo_8S_8(Ale)_4$**.

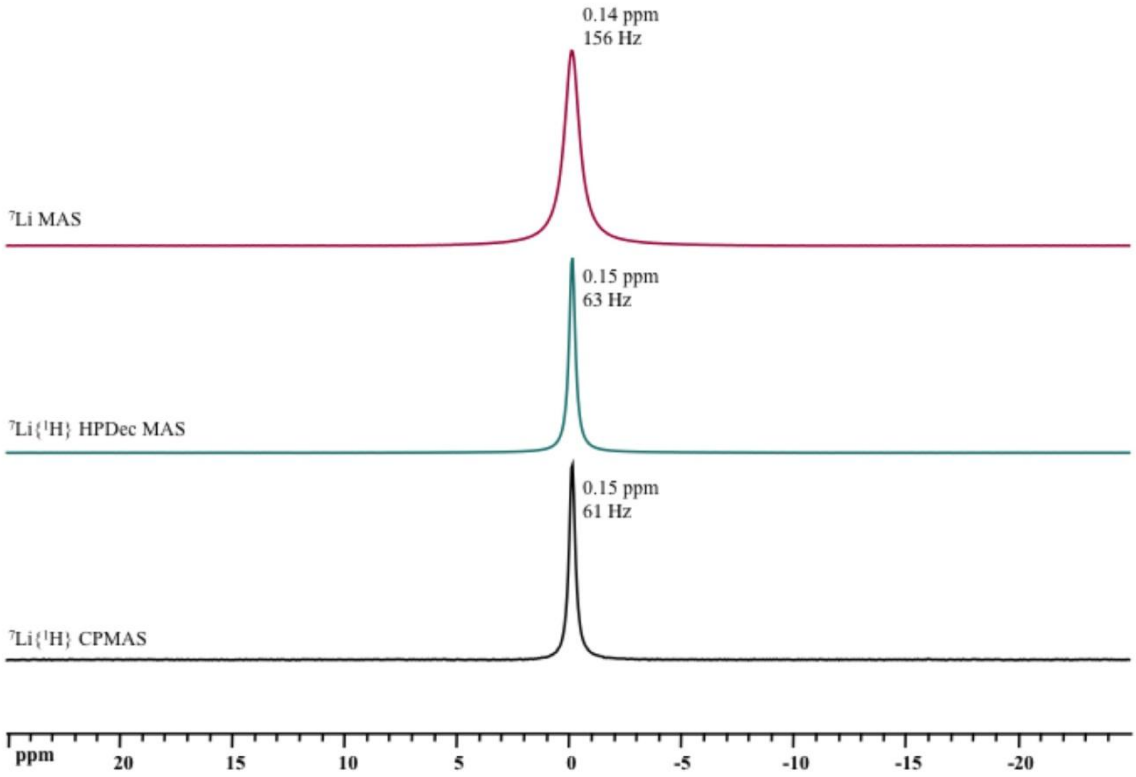

Figure SI8: ^{7}Li MAS NMR spectra of **$Mo_8O_8(Ale)_4$** acquired (top) without CP and heteronuclear decoupling, (medium) without CP but under heteronuclear TPPM decoupling, and (bottom) with CP and heteronuclear TPPM decoupling.

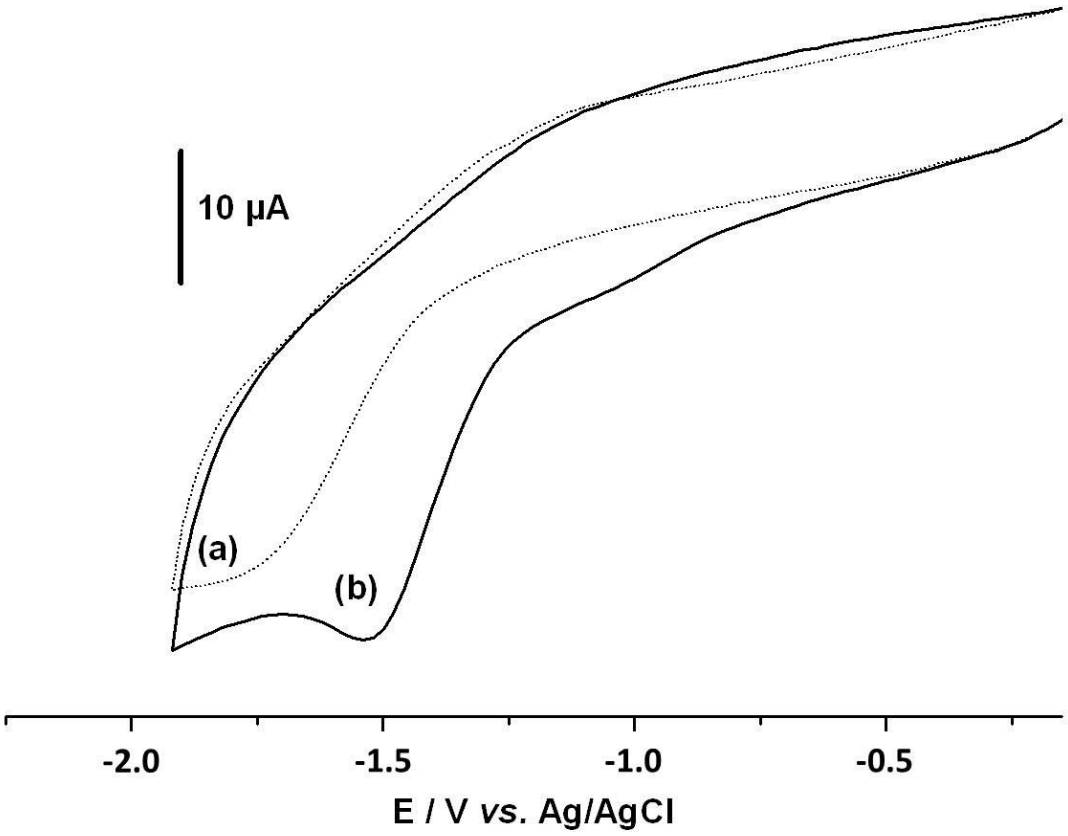

Figure SI9: Cyclic voltammograms of **$Mo_8S_8(Ale)_4$** deposited onto a glassy carbon electrode (b) compared to the bare glassy carbon electrode (a) in CH_3CN + 0.1 M tetrahexylammonium perchlorate as electrolyte in the presence of trifluoroacetic acid 53 µM. Scan rate 0.1 V s^{-1}; potentials are given *vs* AgCl/Ag electrode.